Fast microchannel plate detector with an impedance matched anode in suspended substrate technology

Reto Schletti, Peter Wurz,[a] and Stefan Scherer
Physikalisches Institut, University of Bern, 3012 Bern, Switzerland

Oswald H. Siegmund
Siegmund Scientific, Walnut Creek, California, 94595

(Received 16 October 2000; accepted for publication 4 December 2000)

Fast particle detectors with subnanosecond pulse widths are key elements in modern time-of-flight mass spectrometers. Typically, an impedance matched transmission line from the extended anode to the coaxial cable is necessary to obtain fast pulses. We present an approach using a planar geometry for the transmission line. Thereby, the impedance match is realized with a transition from a 50 Ω suspended substrate microstrip line to a coaxial 50 Ω line. A prototype with an active area of 1.8 cm diameter including a strategy to reduce peak ringing was built and tested. The mean pulse width measured with a 1 GHz analog oscilloscope was 520 ps (full width at half maximum) with a rise time of 380 ps. The robust, compact, and low-weight design of the detector is well suited for an application in space, where weight, space, and power consumption are very limited resources. [DOI: 10.1063/1.1344601]

I. INTRODUCTION

Fast single particle detectors are key elements in time-of-flight (TOF) mass spectrometers. Quite often the mass resolution $m/\Delta m$ is limited by the timing performance of the detector. Therefore, careful design of the detector and detector's electronics within the instrument is required. Additional stringent limitations are imposed on instrumentation on board a spacecraft, where small size, low weight, and low power consumption are important issues. Microchannel-plate (MCP) detectors meet all these requirements and allow for fast timing. Therefore, they are frequently integrated in spaceborne plasma sensors.

Short rise times of detector pulses are required by instrumentation triggering on the leading edge for time to digital conversion. To increase the timing accuracy, constant fraction discriminators are typically used to compensate for the intrinsic variability of the pulse heights originating from MCP detectors. Such a timing strategy is used for TOF spectrometers based on the carbon foil technique[1] commonly used in space plasma research. Thereby, the time a single particle of known kinetic energy needs to travel a certain distance is measured. The mass of the particle is then derived from its velocity. Timing information is obtained from detection of secondary electrons emitted by the particle when crossing a thin carbon foil and from a stop pulse generated by the particle in a detector at the end of the flight path. The mass resolution $m/\Delta m = \tau/2\Delta\tau$ of these linear TOF instruments is limited by energy straggling and angular scattering of the particles in the carbon foil to $\lesssim 30$ for particle energies in the range 1 keV/nucleon to 1 MeV/nucleon. More sophisticated instruments, called isochronous TOF spectrometers, circumvent this problem and achieve resolutions of $m/\Delta m$ up to 100.[2,3] Thereby, ions leaving the carbon foil are deflected in an electrostatic field, which results from a harmonic potential, such that the TOF remains independent of the energy and direction of the ion. The remaining limiting factors are nonideal field configurations and time measurement. For high sensitivity of these sensors, large area detectors are needed. With large area detectors, the capacitance between the anode and the MCP becomes significant and introduces a low pass filter reducing the bandwidth of the electronic circuit.[4] This has to be considered in the design.

Even if only short rise times are needed for exact timing, ringing of the peak might alter measurements with electronics allowing for multiple hits. Also, false triggering after a dead time of the electronics will occur if the pulse arrives just before the TOF window is opened. This leads to ghost peaks in the spectrum. Another positive aspect of short pulses is that larger signal amplitudes are obtained due to the same total charge being collected on the anode in a shorter time. Better signal to noise discrimination is then possible and thus an improvement in the instrument sensitivity results.

Gas and material analysis is a research area where TOF instrumentation is employed more and more in recent years. This results in continuous demand for better performance which means also faster detectors with high fidelity signal transmission. In these applications the fast pulses are not only used for timing, but the pulse form is digitized with the peak area giving a measure of the number of registered ions in the recorded peak. Such an application is the RTOF sensor on the ROSETTA mission where a multireflection TOF mass spectrometer is used to investigate the chemical composition of the comet P/Wirtanen.[5] The present detector was developed primarily for an application in the RTOF sensor. The pulse form and amplitude analysis can also be used to identify ion species according to the number of released second-

[a]Electronic mail: wurz@soho.unibe.ch

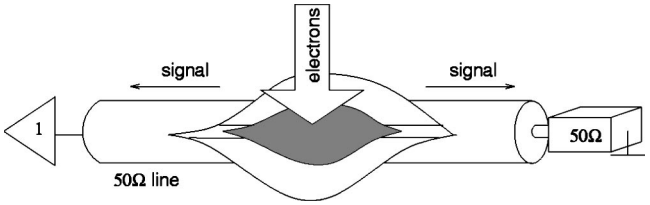

FIG. 1. Working principle: The electron current from the MCPs is injected directly into a 50 Ω transmission line. From there, the electric signal propagates along the line in both directions with a wave resistance of 50 Ω. The wave that propagates toward the terminating 50 Ω resistor is fully absorbed there. The other part propagates toward a remote amplifier and from there to the timing electronics. If parts of the wave are reflected at impedance discontinuities they will be damped at the terminating resistor. No ringing of the pulse will take place, if there is not more than one discontinuity present in the transmission line.

ary electrons upon collision with a converter surface.[6]

In laboratory experiments, the electronics is usually located outside the vacuum chamber. For instrumentation on board a space platform, the detectors are usually located on a high voltage terminal and the TOF electronics is at spacecraft potential. In both cases, the MCP detector and the electronics can be separated by considerable distances which makes a transmission line necessary for pulse propagation. Since laboratory oscilloscopes, amplifiers, and discriminators usually have 50 Ω input resistances, signal transmission is realized with a 50 Ω coaxial cable. To minimize distortion and reflections of the pulse, an impedance matching anode configuration and a broadband electronic circuit are required for transmission of short pulses.

Good results have been obtained in the past with conical transmission lines to match impedance from the extended anode into a coaxial line.[7] A sophisticated modification of the conical anode is the ''Apollonius'' detector,[8,9] where the length of the transition from the anode to a SMA connector could be significantly reduced while maintaining good timing performance for large detector areas. Size and weight of the detector could thus be reduced considerably.

The basic idea for the new detector was to inject the electron current from the MCP directly into a broadened transmission line from the side, as is shown in Fig. 1. A wave packet will hereafter travel along the line in both directions. One end of the line is terminated with a 50 Ω resistor to absorb the arriving pulse without reflections. The other side of the line carries the information to the remote measuring instrumentation. The transition from a large inner conductor serving as anode to a coaxial cable was to be realized in the sense of the Apollonius detector but in a planar geometry using a microstrip line. This concept helps to alleviate two problems encountered with cone matched anodes concerning the stray capacitance between the anode and the MCP. First, this capacitance introduces a low pass filter which limits the bandwidth of the electronic circuit and broadens the pulses. Second, a reflected wave from an impedance discontinuity somewhere on the whole transmission line will charge this capacitance. A second wave will be launched upon discharge of the capacitance and invoke peak ringing, even if the line is terminated on both sides with a 50 Ω resistor. In the new concept, this capacitance is integrated in the transmission line such that no extra capacitance is present.

In microstrip transmission lines, which are widely used in integrated microwave applications, the strip width W scales with the thickness D of the substrate for a given line impedance. For example, with an Al_2O_3 substrate, the W/D ratio is about unity for 50 Ω. This fact does not allow for anodes with dimensions of several centimeters. However, the use of suspended substrate technology allows for considerable larger W/D ratios.

II. THEORY

The propagation of a transverse electromagnetic (TEM) wave of frequency ω in a lossless transmission line is characterized by[10]

$$V(x)=Z_0 I_0(\omega)\, e^{i\omega t}(e^{-ikx}+e^{ikx}) \tag{1}$$

with the impedance Z_0, the wave number k, the voltage at any location along the line $V(x)$, and the amplitude $I_0(\omega)$ of the oscillating current. The impedance, the wave number, and the phase velocity v_p are defined as

$$Z_0=\sqrt{\frac{L'}{C'}},\quad k=\frac{\omega}{v_p},\quad v_p=\frac{1}{\sqrt{L'C'}}=\frac{c}{\sqrt{\epsilon_r}}, \tag{2}$$

where L' and C' are the inductance and the capacitance per unit length of the line, c is the speed of light, and ϵ_r is the relative dielectric constant of the media. The wave propagates in both direction of the transmission line with a phase velocity independent of the frequency of the wave. An initial current pulse

$$I_0(t)=\mathcal{F}^{-1}[I_0(\omega)] \tag{3}$$

is transferred without distortion to the amplifier if no R–C–L filter is introduced which would change the amplitude and the phase of the harmonic wave components.

The well known solution for the impedance Z_0 of a coaxial transmission line is

$$Z_{0,\mathrm{coax}}=\sqrt{\frac{\mu_0}{\epsilon_0}}\frac{1}{2\pi\sqrt{\epsilon_r}}\log\left(\frac{D}{d}\right), \tag{4}$$

where d is the inner and D the outer diameter of the coaxial line, ϵ_r is the relative dielectric constant of the insulation in between, ϵ_0 the vacuum permittivity, and μ_0 the vacuum permeability. The impedance along the line remains constant if the ratio of the outer to the inner conductor remains the same. Thus, the diameter of the inner conductor can be enlarged to fit the size of the MCP area if the outer diameter is enlarged, respectively. The collected electrical current pulse from the MCPs propagates then according to Eq. (1). This is the strategy followed by conical matched anodes, where the inner and the outer conductor have a conic shape, and of the Apollonius detector mentioned in Sec. I. For large area detectors, the diameter of the outer conductor may become too large for a specific application.

The concept of impedance matching can be transferred to a planar geometry using a suspended substrate microstrip transmission line with side walls, for which a cross section is

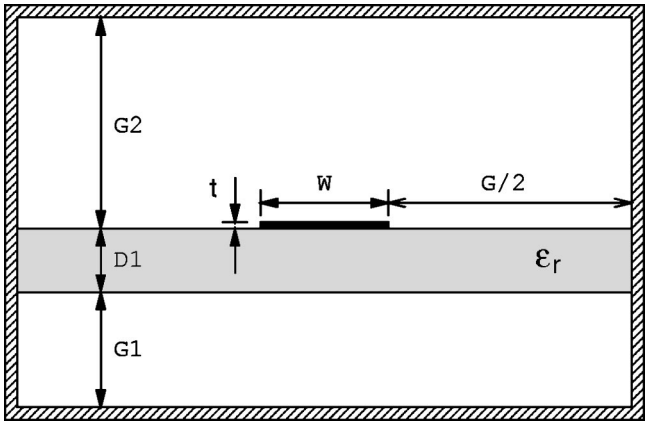

FIG. 2. Cross section of a suspended substrate microstrip transmission line with sidewalls. The dielectric substrate has a thickness $D1$ and a relative dielectric constant ϵ_r. The difference compared to a microstrip line is the gap $G1$ between the dielectric and the backplane. The walls, at distances $G2$ and $G/2$, respectively, are all electrically conducting and screen the strip line from the outside. They have to be taken into account for calculation of the impedance Z_0 of the transmission line. The height t can be neglected in calculations if t is small compared to the width W.

shown in Fig. 2. A conductor of width W is printed on a dielectric substrate of thickness $D1$. The distinction between a suspended substrate and a microstrip line is the gap $G1$ between the substrate and the ground plane. The line is shielded from the outside by two sidewalls and a top plane also at ground potential. The sidewalls have to be taken into account for calculations of Z_0. The height t of the printed conductor can be neglected, if small compared to W.

The propagation mode supported by a microstrip line can not be a pure TEM wave, since the part traveling in the substrate and the part traveling in the vacuum have different phase velocities.[10] However, for $D1 \ll \lambda$ (the wavelength of the wave), the fields are *quasi*-TEM and Eq. (2) translates to

$$v_p = \frac{c}{\sqrt{\epsilon_{r,\mathrm{eff}}}}, \tag{5}$$

where $\epsilon_{r,\mathrm{eff}}$ is the effective dielectric constant and has a value between 1 and ϵ_r. This effective dielectric constant describes the fraction of the wave traveling in the vacuum with respect to the fraction traveling in the substrate. Since the capacitance is proportional to the dielectric constant of the material homogeneously filling the region around the conductor

$$\epsilon_{r,\mathrm{eff}} = C'/C'_0, \tag{6}$$

where C'_0 is the capacitance per unit length of the line with ϵ_r set to 1 (vacuum). The impedance Z_0 of the stripline is then

$$Z_0 = \sqrt{\frac{L'}{C'}} = \frac{\sqrt{\epsilon_{r,\mathrm{eff}}}}{c\,C'} = \frac{1}{c\,\sqrt{C'C'_0}}, \tag{7}$$

and can be calculated from C' and C'_0 only.

The capacitance of a two-dimensional electric field can be calculated solving Poisson's equation with help of the conformal mapping technique. This method was used in Ref. 11, where the even- and the odd-mode capacitance of coupled suspended substrate lines was calculated. The contribution of the sidewalls (E walls) to the capacitance can be simulated using the odd-mode capacitance of two lines separated by a distance which is twice as large as the wall distance. The total C' is

$$C' = 2C'_p + 4C'_{\mathrm{fo}}, \tag{8}$$

where

$$2C'_p = \frac{\epsilon_0 W}{G2} + \frac{\epsilon_0 W}{G1 + (1/\epsilon_r)\,D1} \tag{9}$$

is the parallel component and the four C'_{fo} are the fringing odd-mode components of the capacitance. The value of C'_0 is calculated accordingly. The impedance Z_0 of a suspended substrate can therefore be interpreted as function

$$Z_0 = f(W, G1, D1, G2, G, \epsilon_r). \tag{10}$$

If $D1$, $G2$, $G+W$, and ϵ_r remain constant along the transmission line, the impedance is a function of the width W and of the gap $G1$ only. These two parameters can be modified very easily along a strip line.

III. DESIGN

We designed a prototype of a detector for the RTOF sensor of the ROSINA[5] instrument on the ROSETTA mission of the European Space Agency (ESA). The detector was designed with a floating anode, since the front surface of the MCP stack was required to be at a given high voltage. The dimensions of the detection unit (length L and width $G+W$ of the anode housing) were given by the available space in the RTOF sensor, as well as by the size of the MCPs.

The MCP stack is built with two MCPs (Photonis G6-2S SE/6, $L/D=55$, 6 μm pores, 25 mm outer diameter, 40 MΩ each, $\pm 10\%$ matched) in matched pair configuration. A high transmission grid (95%, etched Mo, Au plated) terminates the anode housing at a distance of 2 mm from the backsurface of the second MCP. An acceleration potential of 600 V is set up between the MCP exit and the grid, to accelerate the electrons over this short distance. The grid was included because the gap $G2$ had to be chosen large enough to allow for a large width W of the line. A long accelerating path for the electrons would broaden the peak due to differences in electron TOF. The anode potential is supplied directly through the terminating 50 Ω resistor (see Fig. 3) and equals the grid potential as well as the potential of the inner walls of the housing. The space inside the housing is therefore field-free and no deflection of the electron trajectories takes place.

As dielectric substrate we used a 1-mm-thick Al_2O_3 (96%) ceramic plate because of its ultrahigh vacuum compatibility. The anode metallization is gold plated copper. The terminating resistor is a surface mounted device (SMD) type soldered onto the metallization and onto the housing structure. The capacitive decoupling of the signal was realized using a discrete SMD high voltage condenser (440 pF, KD Components). Lower values of this capacitance imply a higher cutoff frequency of the high pass filter defined by the condenser and two 50 Ω resistors, which leads to deforma-

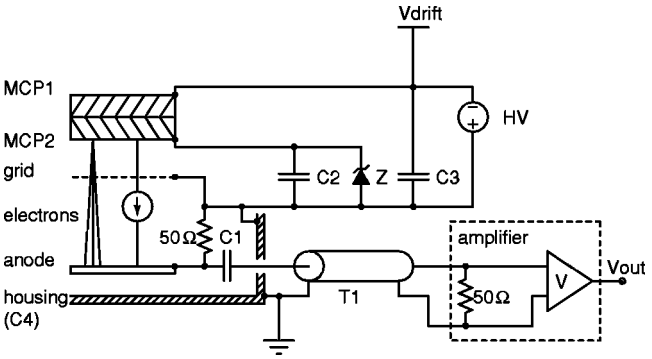

FIG. 3. Schematic of the electronic circuit of the detector. The electron current pulse from the MCP is collected on the anode. The anode potential is supplied directly by the terminating 50 Ω resistor inside the housing. The decoupling capacitance C_1, the termination resistor, and the 50 Ω resistor of the amplifier define a high pass filter. The value of C_1 has to be chosen not to limit the bandwidth of the circuit. The resistance of the MCP stack is $\simeq 80$ MΩ. The acceleration potential $U_Z = 600$ V between the MCP backside and the grid is supplied with two Zener diodes in series. The capacitance C_2 is needed to replace the charge released from the MCP by the electron avalanche and to keep the potential of the MCPs constant during the pulse. The capacitors C_3 and C_4, which is built up by the anode housing dielectrics, ensure for proper HF signal return.

tions of the peak shape due to phase shifts. Its value (as low as possible) was selected from transient analysis of the electrical circuit shown in Fig. 3 using Berkeley SPICE3.[12] The high frequency performance of the decoupling condenser (the capacitance is needed only at low frequencies) is assured by the small size of the SMD component and the absence of inductive supply wires. The connection to the coaxial line is realized with a 50 Ω subminiature-A (SMA) connector (MACOM) integrated in the anode housing. The housing has several functions. It provides the supporting structure for the MCPs, the grid, the anode, and the SMA connector. Furthermore, it acts as external conductor of the transmission line and as an electronic shield. Since the inside of the housing is biased to anode potential, the ground return has to be coupled capacitively (see Fig. 3 capacitor $C4$). All these requirements were achieved using a housing manufactured in 30% glass filled polyetheretherketone (PEEK), which is a semicrystalline, high temperature engineering thermoplastic, metallized inside and outside. The housing cover, supporting the MCPs is made of aluminum. In the flight version the housing cover is made of Au plated titanium, as well as the anode backplane.

During operation, high voltage breakdowns can damage sensitive electronic components like preamplifiers. Such an event occurring on board a space platform may render a whole instrument unusable and is often the cause for sensor failures. The MCP power supply circuit (see Fig. 3) helps to protect the subsequent electronic devices, notably the preamplifier, due to decoupled signal and HV supply circuits introduced by the anode housing biased to HV.

As seen in Eq. (10), the impedance of the transmission line is a function of W and $G1$ only if the other parameters remain constant. The total width $(G+W)$ and the total length L were given by the available space in the sensor. $D1$ and ϵ_r were given by the chosen substrate. We first calculated a set for the parameters $G1_{\max}$ and $G2$ to yield an impedance of 50 Ω in the center of the detector with a width W of the anode corresponding to the diameter of the MCP stack just above it. The full parameter set is shown in Table I. We set the gap $G1_{\min}=0$ at the boundary of the substrate (microstrip line) to interface the SMD components.

TABLE I. Parameter set for the prototype MCP detector.

Parameter	value	unit
Z_0	50	Ω
ϵ_r	9.5	
$D1$	1.0	mm
L	60.0	mm
$G2$	7.0	mm
$G+W$	36.2	mm
$W_{\max}$	19.6	mm
$G1_{\max}$	10.0	mm
$W_{\min}$	1.0	mm
$G1_{\min}$	0.0	mm

The transition of the gap $G1$, from $G1_{\max}$ to $G1_{\min}$ was chosen to follow

$$G1(\hat{x}) = G1_{\max}\begin{cases} \hat{x}^3(-3\hat{x}+4) & \text{for } 0 \leqslant \hat{x} \leqslant 1 \\ (2-\hat{x})^3(3\hat{x}-2) & \text{for } 1 < \hat{x} \leqslant 2 \end{cases}, \quad (11)$$

where $\hat{x}=2x/L$ is a normalized coordinate. This function has three points of inflection (where first and second derivative vanish), namely at $\hat{x}=0$, at $\hat{x}=1$, and at $\hat{x}=2$. The equation for the impedance

$$Z_0[W(\hat{x}), G1(\hat{x})] - 50 = 0 \quad (12)$$

was numerically solved for $W(\hat{x})$ using Newton's method. The solution is shown in Fig. 4. The shape of the anode metallization (Au) printed on the Al_2O_3 substrate is shown together within the boundaries of the anode housing. The

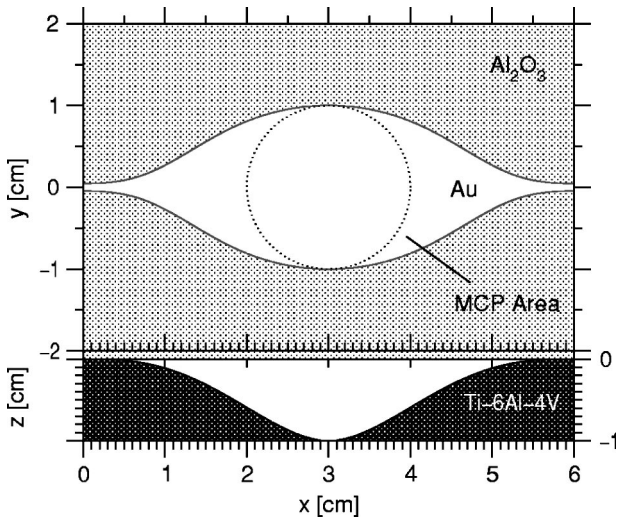

FIG. 4. Schematics of the anode (upper panel) and of the backplane (lower panel) of the detector. The top panel ($x-y$ plane) represents the Al_2O_3 substrate (light gray) and the printed Cu/Au anode inside the anode housing (figure axes). The MCP area is indicated with a dotted circle. The lower panel ($x-z$ plane) represents the Ti–6Al–4V backplane (dark gray) as calculated from Eq. (11) and the Al_2O_3 substrate on top of it (light gray). A SMD terminating 50 Ω resistor is placed at one end of the printed anode, and a SMD capacitance followed by a SMA connector at the other end.

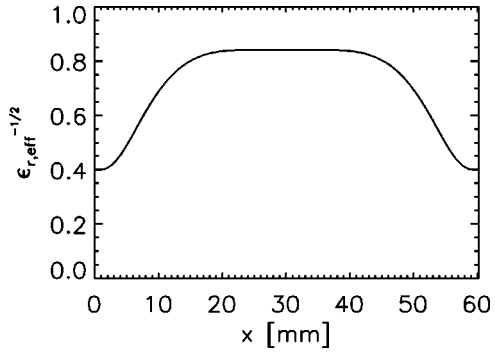

FIG. 5. Relative phase velocity $v_p/c=(\epsilon_{r,\mathrm{eff}})^{-1/2}$ of the *quasi*-TEM wave along the transition from the suspended substrate line (in the center) to the microstrip line at $x=0$ and $x=60$ mm for the prototype detector.

size and the position of the MCP stack are indicated by the dotted line. The lower panel shows the backplane ($G1$) following Eq. (11).

In Fig. 5 we plot the value of $1/\sqrt{\epsilon_{r,\mathrm{eff}}}$ as a function of $\hat{x}$, which represents the ratio of the phase velocity of the *quasi*-TEM wave to the speed of light c. In the center of the detector, its value is $0.84\,c$, indicating that a large fraction of the field lines of the wave is located in the vacuum. Here, the effects of the side walls are not negligible. This implies a design which integrates the grid into the housing to maintain a constant gap $G2$. At the end of the transmission line, where the gap $G1$ is small and the line becomes more and more a microstrip line, most of the field lines are concentrated in the dielectric substrate. The speed of the wave decreases to $0.4\,c$. The propagation time of a wave from one end of the anode to the other is 300 ps (integrated from Fig. 5). Note that the wave speed is higher at the location where the charge falls onto the stripline. This results in a low transient time spread of ~30 ps full width at half maximum (FWHM).

A photography of the constructed prototype is shown in Fig. 6. The weight of the whole assembly is only 94 g.

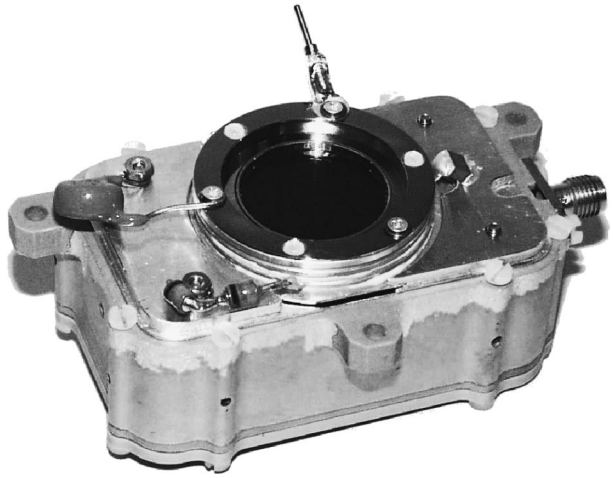

FIG. 6. Photograph of the integrated prototype. The front MCP is visible as well as the Zener diodes and the condenser C_2 (right side) and C_3 (left side). The PEEK housing, metallized inside and outside, provides the return capacitor C_4. On the right side, the SMA connector can be seen.

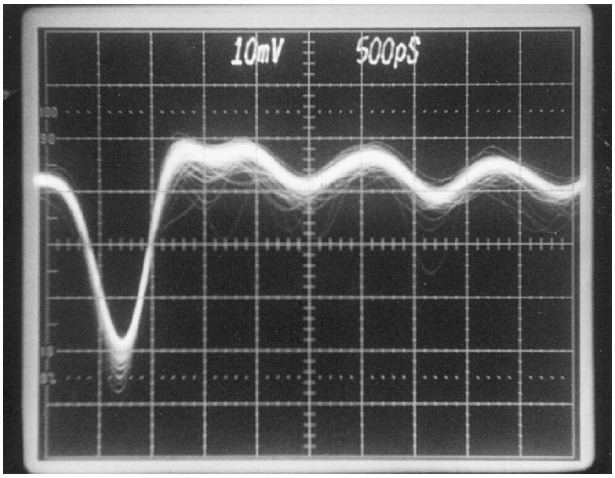

FIG. 7. Oscilloscope trace of a set of pulses recorded with a 1 GHz analog oscilloscope.

IV. MEASUREMENTS

The measurement setup consists of an analog oscilloscope (Tectronix, model 7104) with a bandwidth of 1 GHz and a rise time of 350 ps. The detector was connected inside the vacuum with a 1 m Ti semirigid coaxial cable (Kaman) to a 50 Ω HF coaxial vacuum feedthrough. Outside, a 50 Ω coaxial cable (Huber and Suhner) was connected to the 50 Ω input of the oscilloscope. Figure 7 shows the trace of a series of pulses recorded with the analog oscilloscope.

The measured pulse width was 520 ps (FWHM) and the rise time was 380 ps. A significant fraction of the pulse width[9] has to be attributed to the limited bandwidth of the oscilloscope, which introduces a low pass filter into the transmission line. The real signal rise time can be approximated with

$$\tau_{\mathrm{rise,real}}\approx\sqrt{\tau_{\mathrm{rise,meas}}^2-\tau_{\mathrm{rise,scope}}^2}\approx 150\ \ \mathrm{ps}. \tag{13}$$

The raw pulse width obtained with the Appollonius detector[9] with the same analog scope was 580 ps. The pulse width after correction of the bandwidth of the measurement electronics of the conical detector[7] was 750 ps. The electrical performance is influenced by some critical elements in the design. The placement of the condenser C_2 and C_3 as well as the return condenser C_4, which is integrated in the housing, influence the peak shape to some extend. Especially the oscillations after the peak are sensitive to the placement of these elements. The decoupling condenser and the Zenner diodes are of minor importance for these effects. Details of the electrical performance parameters such as pulse height distributions, gain, background rates, and thermal characteristics, are presented in Ref. 13.

ACKNOWLEDGMENTS

The authors are grateful to APCO Technologies SA, Vevey, Switzerland supporting the development of the detector for use in the RTOF sensor on the ROSETTA mission. This work was supported by the Swiss National Science Foundation and the PRODEX program of ESA.

[1] G. Gloeckler and K. C. Hsieh, Nucl. Instrum. and Methods **165**, 537 (1997).
[2] D. C. Hamilton, G. Gloeckler, F. M. Ipavich, R. A. Lundgren, R. B. Sheldon, and D. Hovestadt, Rev. Sci. Instrum. **61**, 3104 (1990).
[3] L. Gubler, P. Wurz, P. Bochsler, and E. Moebius, Int. J. Mass Spectrom. Ion Processes **148**, 77 (1995).
[4] R. Schletti, Ph.D. thesis, University of Bern, Switzerland, 2000.
[5] H. Balsiger *et al.*, ESA SP-1165 (in press).
[6] D. G. Mitchell *et al.*, Opt. Eng. **32**, 3096 (1993).
[7] J. L. Wiza, Nucl. Instrum. Methods **162**, 587 (1979).
[8] P. Wurz and L. Gubler, Rev. Sci. Instrum. **65**, 871 (1994).
[9] P. Wurz and L. Gubler, Rev. Sci. Instrum. **67**, 1790 (1996).
[10] D. M. Pozar, in *Microwave Engineering*, 2nd ed., edited by C. Robey (Wiley, New York, 1998).
[11] J. I. Smith, IEEE Trans. Microwave Theory Tech. **MTT–19**, 424 (1971).
[12] T. Quarles, A. R. Newton, D. O. Pederson, and A. Sangiovanni-Vincentelli, *SPICE3 Version 3f User's Manual*, University of California, Berkeley, 1993.
[13] O. H. W. Siegmund, K. Kromer, P. Wurz, R. Schletti, and H. Cottard, Proc. SPIE **4140** (2000) (in press).